POLITECNICO DI TORINO
Repository ISTITUZIONALE

Current-Based Synthesis of Beam Switching Metasurface Antennas

Original
Current-Based Synthesis of Beam Switching Metasurface Antennas / Samadzadehghezelghayeh, S., Teodorani, L., Zucchi, M., Vecchi, G.. - (2026), pp. 1-4. (20th European Conference on Antennas and Propagation (EuCAP 2026) Dublin (Ire) 19-24 April 2026) [10.23919/eucap68105.2026.11612068].

Availability:
This version is available at: 11583/3014941 since: 2026-09-25T13:18:16Z

Publisher:
IEEE

Published
DOI:10.23919/eucap68105.2026.11612068

Terms of use:

This article is made available under terms and conditions as specified in the corresponding bibliographic description in the repository

Publisher copyright
IEEE postprint/Author's Accepted Manuscript

©2026 IEEE. Personal use of this material is permitted. Permission from IEEE must be obtained for all other uses, in any current or future media, including reprinting/republishing this material for advertising or promotional purposes, creating new collecting works, for resale or lists, or reuse of any copyrighted component of this work in other works.

(Article begins on next page)

26 November 2026

Current-Based Synthesis of Beam Switching Metasurface Antennas

Shaghayegh Samadzadehghezelghayeh*, Lucia Teodorani*, Marcello Zucchi†, Giuseppe Vecchi*
*Department of Electronics and Telecommunications, Politecnico di Torino, Turin 10129, Italy, lucia.teodorani@polito.it
†Advanced Computing, Photonics & Electromagnetics (CPE) area, Fondazione LINKS, Turin 10138, Italy

***Abstract*—We extend the current-based metasurface synthesis of tensorial surface impedance to demonstrate *beam switching* with multiple feeds and one-beam-per-feed. The process optimizes the surface current (as opposed to impedance), and impedance determination is carried out as a post-processing. The cost functional encodes tensor-impedance passivity and realizability, and far-field masks. To achieve beam switching, we add a functional enforcing pairwise cross-testing constraints among all excitations to ensure co-existence of multiple currents on the same aperture due to different feeds. The resulting current-only problem is solved with a nonlinear conjugate-gradient method featuring a closed-form line search, and the optimized tensor impedance is realized using unit cells ad-hoc selected from a database of precomputed geometries.**

I. Introduction

Metasurface antennas comprise electrically thin, planar arrays of subwavelength unit cells that sculpt aperture fields and radiation patterns with fine spatial resolution [1]. The associated design task is inherently large scale—each cell contributes one or more controllable parameters—so accuracy and computational efficiency are both critical.

We model the aperture via an Impedance Boundary Condition (IBC) and explicitly synthesize *tensorial* (anisotropic) sheet impedances. Anisotropy increases control over the conversion of bound surface waves into leaky radiation, which in practice correlates with improved efficiency, reduced sidelobes, and higher gain [2], [3]. In line with recent formulations that target tensor impedances directly [4], [5], our work builds on a current-based framework [6] extended to realistic feeding [7]. The optimization variable is the surface current, and all requirements are encoded as functionals of that current.

This paper addresses *passive multi-feed beam switching* on a *single, fixed aperture*; beam reconfigurability is a necessary feature in modern telecommunication systems [8]. Multiple feeds are embedded in the same structure; each feed is designed to excite one predetermined beam, and the scan is realized by selecting the active feed (no tunable components or biasing). To ensure that the shared tensor-impedance sheet guarantees the co-existence of feeds, we introduce pairwise cross-testing constraints. Let $R_{pq} := \langle \mathbf{J}_p, \mathbf{E}_q \rangle$ denote the "correlation" between the equivalent current due to feed p and the electric field produced by feed q; we enforce $R_{pq} = R_{qp}$ for all $p \neq q$, which ensures consistency across feeds while remaining compatible with the current-only formulation. The composite objective function comprises (i) realizability/passivity terms and pairwise cross-testing constraints to ensure consistency of all feeds on the shared metasurface. (ii) far-field penalties enforcing masks on beam-width, side-lobes, and cross-polarization. The resulting polynomial structure enables a nonlinear conjugate-gradient (NLCG) solver with a closed-form line search for rapid iterations at scale. After optimization, the synthesized tensor pattern is realized using anisotropic unit cells drawn from a precomputed database; rotation of the unit cells sets the anisotropy orientation [6], [9].

II. Metasurface with Multiple Feeds

Consider a tensor metasurface (MTS) excited by multiple feeds f_n, $n = 1, \ldots, N_f$, placed at distinct locations and independently excitable. Let $\{\mathbf{E}_{tn}, \mathbf{J}_n\}$ denote the tangential electric field and the equivalent surface current on the MTS when only f_n is active. These quantities are related by the (position-dependent) surface-impedance tensor. Since all beams must be produced by the same physical sheet, the impedance pattern must be identical for all excitations; equivalently,

$$\boldsymbol{E}_{\mathrm{t}n}(\boldsymbol{r}) = \overline{\overline{\boldsymbol{Z}}}(\boldsymbol{r}) \cdot \boldsymbol{J}_n(\boldsymbol{r}), \qquad n = 1, ..., N_f \tag{1}$$

with $\overline{\overline{\boldsymbol{Z}}} = \mathrm{j}X_{\mathrm{I}}\,\overline{\overline{\boldsymbol{I}}} + \mathrm{j}X_{\mathrm{K}}\,\overline{\overline{\boldsymbol{K}}} + \mathrm{j}X_{\mathrm{L}}\,\overline{\overline{\boldsymbol{L}}}$ being the purely reactive impedance tensor of the *passive* and *lossless* MTS [10]. The basis dyadics $\overline{\overline{\boldsymbol{I}}}$, $\overline{\overline{\boldsymbol{K}}}$ and $\overline{\overline{\boldsymbol{L}}}$, expressed in the Cartesian coordinate basis $(\hat{\boldsymbol{x}}, \hat{\boldsymbol{y}})$, are given by:

$$\overline{\overline{\boldsymbol{I}}} = \hat{\boldsymbol{x}}\hat{\boldsymbol{x}} + \hat{\boldsymbol{y}}\hat{\boldsymbol{y}}, \tag{2}$$

$$\overline{\overline{\boldsymbol{K}}} = \hat{\boldsymbol{x}}\hat{\boldsymbol{x}} - \hat{\boldsymbol{y}}\hat{\boldsymbol{y}}, \tag{3}$$

$$\overline{\overline{\boldsymbol{L}}} = \hat{\boldsymbol{y}}\hat{\boldsymbol{x}} + \hat{\boldsymbol{x}}\hat{\boldsymbol{y}}. \tag{4}$$

Because the impedance pattern is common to all excitations, we can perform pairwise cross-tests of (1) for any feed pair (p, q):

$$\langle\, \boldsymbol{J}_p \,, \boldsymbol{E}_{\mathrm{t}q} \,\rangle = \langle\, \boldsymbol{J}_p \,, \overline{\overline{\boldsymbol{Z}}}(\boldsymbol{r}) \cdot \boldsymbol{J}_q(\boldsymbol{r}) \,\rangle, \quad p, q = 1, ..., N_f, \tag{5}$$

with $\langle\, \boldsymbol{a} \,, \boldsymbol{b} \,\rangle$ indicating the symmetric bilinear form

$$\langle\, \boldsymbol{a} \,, \boldsymbol{b} \,\rangle = \frac{1}{A_\Sigma} \int_\Sigma \boldsymbol{a} \cdot \boldsymbol{b}\, \mathrm{d}S, \tag{6}$$

where Σ is the surface of interest and A_Σ is its area. Developing the products on the right hand side of (5) shows that every "correlation" integral $R_{pq} := \langle\, \boldsymbol{J}_p \,, \boldsymbol{E}_q \,\rangle$ is equal to its reciprocal, i.e.,

$$\langle\, \boldsymbol{J}_p \,, \boldsymbol{E}_{\mathrm{t}q} \,\rangle = \langle\, \boldsymbol{J}_q \,, \boldsymbol{E}_{\mathrm{t}p} \,\rangle, \qquad p, q = 1, ..., N_f. \tag{7}$$

Thus, enforcing (7) for every feed pair (p, q) guarantees the co-existence of the associated fields $\{\boldsymbol{E}_{\mathrm{t}p}, \boldsymbol{J}_p\}, \{\boldsymbol{E}_{\mathrm{t}q}, \boldsymbol{J}_q\}$ on the same passive and lossless MTS; accordingly, (7) constitutes the additional constraint that the current-based synthesis must impose to accommodate multiple feeds on a passive, lossless metasurface.

III. Current-Based IBC Synthesis

Within the current-only metasurface synthesis framework of [6], [7], [9], the algorithm minimizes a total cost function that can be written as

$$f = f_{\mathrm{rad}} + f_{\mathrm{ibc}} + f_{\mathrm{pec}}, \tag{8}$$

where each term is a functional of the surface current *only*. Specifically, f_{rad} encodes the radiated–field specifications (e.g., beam-width, side-lobes, cross–polarization), f_{ibc} enforces realizability constraints on the IBC region, and f_{pec} imposes the PEC condition used to model realistic feeding structures [7].

As explained in Section II, in order to expand this method to deal with a multi-feed, multi-beam environment, a new functional f_{mf} enforcing (7) must be added to the objective function (8) to be minimized:

$$f_{\mathrm{mf}} = \sum_{p,q} \left| R_{pq} - R_{qp} \right|^2 . \tag{9}$$

These constraints must be evaluated locally on the MTS; specifically, the surface is meshed with a triangular tessellation, and the EFIE-IBC forward problem is discretized following the Method of Moments approach with Galerkin testing and L Rao-Wilton-Glisson (RWG) basis functions $\boldsymbol{\Lambda}_l$ [11]. When dealing with multiple feeds, the array of unknown current coefficients that the algorithm aims to optimize consists of the concatenation of coefficients of all surface currents:

$$\mathsf{I} = [\mathsf{I}_1; ...; \mathsf{I}_{N_f}], \tag{10}$$

where, for every $n = 1, ..., N_f$,

$$\boldsymbol{J}_n = \sum_l I_{n,l}\, \boldsymbol{\Lambda}_l, \qquad\qquad l = 1, ..., L. \tag{11}$$

Therefore, the total number of unknown is $N = N_f \cdot L$.

The far-field mask-type constraints are set independently on each set of currents, according to the desired pattern and polarization, in the same way as in the case of a single feed outlined in [6]. On the other hand, the strategy for enforcing the tensor impedance realizability constraints introduced in [9] must be adapted to a multi-feed scenario; specifically, the impedance components X_{I}, X_{K} and X_{L} must be expressed as functions of all sets of fields coexisting on the MTS. Similarly to the procedure outlined in [9], we cross-test (1) for every feed $p = 1, ..., N_f$ against the testing functions $\boldsymbol{\tau}_{\mathrm{T}q}(\boldsymbol{r}) = \overline{\overline{\boldsymbol{T}}} \cdot \boldsymbol{J}_q^*(\boldsymbol{r})$, with $\overline{\overline{\boldsymbol{T}}}$ being equal to $\overline{\overline{\boldsymbol{I}}}$, $\overline{\overline{\boldsymbol{N}}}$, $\overline{\overline{\boldsymbol{K}}}$ or $\overline{\overline{\boldsymbol{L}}}$, for every other $q = 1, ..., N_f$. After some calculations, we find the following expressions for X_{I}, X_{K} and X_{L}:

$$X_{\mathrm{I}} = -P_{\mathrm{N}} / \mathcal{J}_{\mathrm{N}}, \tag{12}$$

$$X_{\mathrm{K}} = -P_{\mathrm{L}} / \mathcal{J}_{\mathrm{N}}, \tag{13}$$

$$X_{\mathrm{L}} = P_{\mathrm{K}} / \mathcal{J}_{\mathrm{N}}, \tag{14}$$

where

$$P_{\mathrm{N}} = \mathrm{Re}\Big\{ \sum_{p,q} \Big[\langle\, \boldsymbol{J}_p^*\,, \overline{\overline{\boldsymbol{N}}} \cdot \boldsymbol{E}_{\mathrm{t}q} \,\rangle + \langle\, \boldsymbol{J}_q^*\,, \overline{\overline{\boldsymbol{N}}} \cdot \boldsymbol{E}_{\mathrm{t}p} \,\rangle \Big] \Big\}, \tag{15}$$

$$P_{\mathrm{K}} = \mathrm{Re}\Big\{ \sum_{p,q} \Big[\langle\, \boldsymbol{J}_p^*\,, \overline{\overline{\boldsymbol{K}}} \cdot \boldsymbol{E}_{\mathrm{t}q} \,\rangle + \langle\, \boldsymbol{J}_q^*\,, \overline{\overline{\boldsymbol{K}}} \cdot \boldsymbol{E}_{\mathrm{t}p} \,\rangle \Big] \Big\}, \tag{16}$$

$$P_{\mathrm{L}} = \mathrm{Re}\Big\{ \sum_{p,q} \Big[\langle\, \boldsymbol{J}_p^*\,, \overline{\overline{\boldsymbol{L}}} \cdot \boldsymbol{E}_{\mathrm{t}q} \,\rangle + \langle\, \boldsymbol{J}_q^*\,, \overline{\overline{\boldsymbol{L}}} \cdot \boldsymbol{E}_{\mathrm{t}p} \,\rangle \Big] \Big\}, \tag{17}$$

$$\mathcal{J}_{\mathrm{N}} = \mathrm{Im}\Big\{ \sum_{p,q} \Big[\langle\, \boldsymbol{J}_p^*\,, \overline{\overline{\boldsymbol{N}}} \cdot \boldsymbol{J}_q \,\rangle + \langle\, \boldsymbol{J}_q^*\,, \overline{\overline{\boldsymbol{N}}} \cdot \boldsymbol{J}_p \,\rangle \Big] \Big\}. \tag{18}$$

The tensor impedance constraints are then enforced with the same functionals as in [9]. The tensor impedance pattern computed from the optimized currents can be implemented by selecting a suitable anisotropic unit cell from a precomputed database [9].

IV. Results

The prototype is a circular metasurface designed at $f = 38.5$ GHz with radius of $R = 78$ mm $\approx 10\lambda_0$ (where λ_0 is the free-space wavelength at 38.5 GHz). It is implemented on a grounded Rogers RO3003 substrate with relative permittivity $\varepsilon_r = 3.0$ and thickness $h = 0.635$ mm. The excitation is modeled as the fundamental TM_0 cylindrical surface wave supported by the grounded substrate, which captures the dominant contribution from practical feeds (e.g., a vertical probe/pin) to the launched tangential electric field over the metasurface.

Our experiments demonstrate the coexistence of multiple beams on a single passive aperture, enabling passive beam switching, in two scenarios: (i) multi-beam with *separated* beams for discrete switching, and (ii) multi-beam with *overlapping* beams to support continuous beam coverage.

The first experiment demonstrates a multi-beam configuration with two separated beams, generated by two feeds spaced by $8\lambda_0$ center-to-center on the metasurface. One feed is designed to produce a squinted beam at $\theta = -30°$, while the other generates a broadside beam. As shown in Fig. 1, the synthesized tensor-impedance distribution yields two clearly separated beams excited by their respective sources. The realized surface current and the realized impedance distribution are shown in Figs. 2 and 3, respectively. The realized peak gain is about 31 dB for both beams, and the first sidelobe for squinted beam lies 19 dB below the peak. This value for the broadside beam is 25 dB below. The aperture efficiency is 33% for the squinted beam and 34% for the broadside beam.

The second experiment realizes multibeam with two overlapping beams for continuous coverage in beam switching. we evaluate the feasibility of closely spaced beams with sufficient

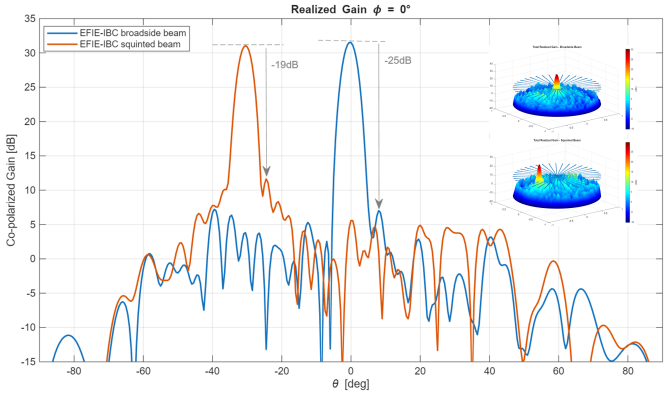

Fig. 1. Separated beams: realized gain pattern in the plane $\phi = 0^\circ$ for two feed sources, generating a squinted beam at -30°, and the other at broadside.

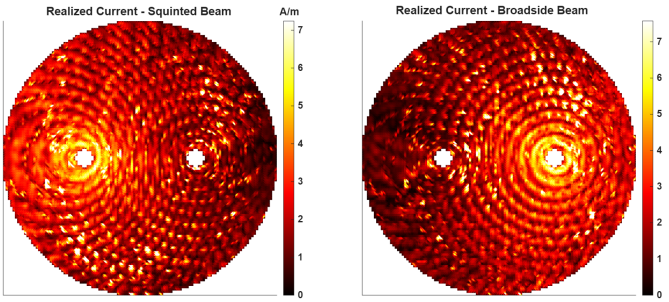

(a) (b)

Fig. 2. (a) Surface current for squinted beam at -30° (b) Surface current for broadside beam

overlap (the usual -3 to -5dB crossing point [12]). In view of providing several beams and thus separated feed points, we have introduced a rectangular slot in the metasurface to enable repositioning of the feed sources. In this experiment, two closely spaced beams were designed with the feeds placed at a center-to-center spacing of $1\lambda_0$, and the patterns were specified to intersect at -5 dB. As shown in Fig. 4, reducing the feed separation and introducing the slot limits the degrees of freedom in the impedance pattern, which results in elevating sidelobe levels. The resulting surface current for one feed, in the presence of the second, is reported in Fig. 5, while Fig. 6 shows the corresponding synthesized tensor-impedance distribution.

The maximum realized gain of beams is 30 dB for broadside, and 31 dB for squinted beam. The aperture efficiencies of the squinted and broadside beams are 22% and 24%, respectively. The reduction of aperture efficiency with respect to the previous experiment is attributed to the slot. To obtain clean separation between closely spaced beams, a good initialization of the surface current is essential. Our procedure is: (i) independently optimize the metasurface current and synthesize the (tensor) impedance for each target beam; (ii) compute the geometry-aligned average of the resulting impedance maps; and (iii) solve the EFIE on this averaged sheet (with the intended multi-feed excitation) to generate the initial currents

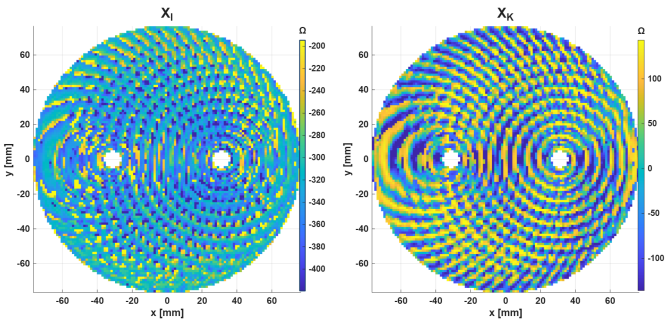

(a) Surface impedance X_I (b) Surface impedance X_K

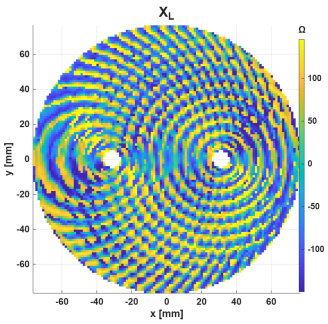

(c) Surface impedance X_L

Fig. 3. Synthesized surface tensor components of the circular MTS antenna radiating a circularly polarized broadside beam and a squinted beam at -30°, with a rectangular slot used to position multiple feeds for beam scanning.

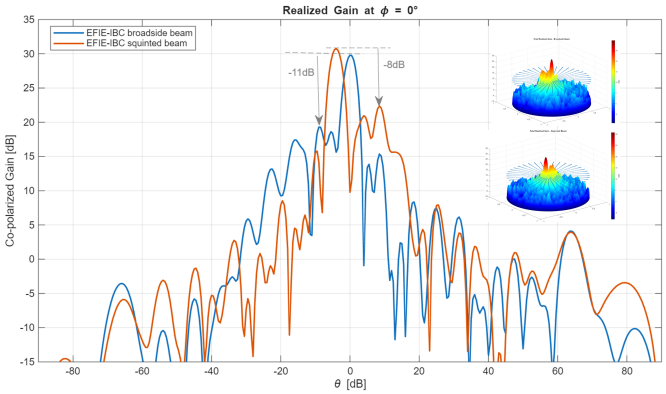

Fig. 4. Overlapping beams: realized gain pattern in the plane $\phi = 0^\circ$ for two feed sources generating a squinted beam at -4°, and at broadside.

for the joint optimization.

V. Conclusions

In this work, we extend a current-based synthesis of tensor metasurfaces to enable *passive beam switching* with multiple coexisting feeds, where switching is performed by exciting a selected feed on a single fixed aperture. We verify two cases: (i) multi-beam with separated beams for discrete switching, and (ii) multi-beam with overlapping beams to support continuous switching. Demonstrations on a circular metasurface producing a pencil beam and a squinted beam confirm the efficacy of the proposed method.

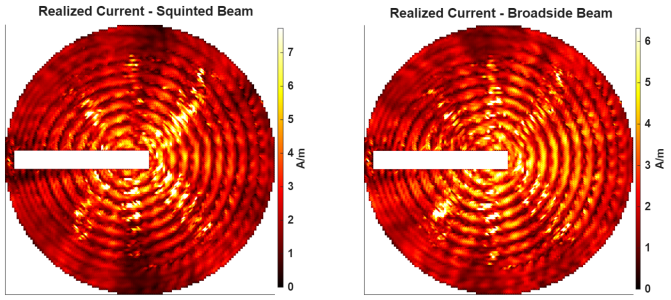

(a) (b)

Fig. 5. (a) Surface current for squinted beam at -4° (b) Surface current for broadside beam

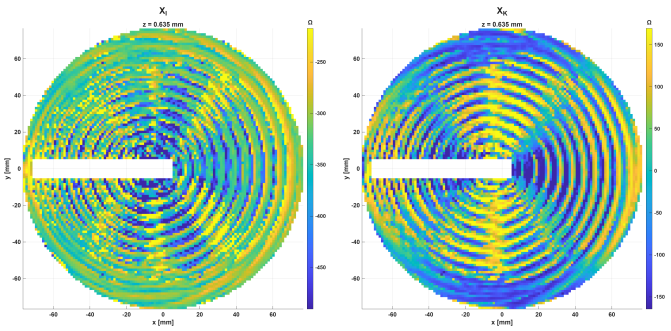

(a) Surface impedance X_I (b) Surface impedance X_K

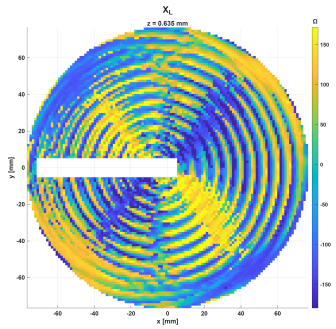

(c) Surface impedance X_L

Fig. 6. Synthesized surface tensor components of the circular MTS antenna radiating a circularly polarized broadside beam and a squinted beam at -4°, with a rectangular slot used to position multiple feeds for beam scanning.

ACKNOWLEDGMENT

This work was supported by the European Union - Next Generation EU under the Italian National Recovery and Resilience Plan (NRRP), Mission 4, Component 2, Investment 1.3, CUP E13C22001870001, partnership on "Telecommunications of the Future" (PE00000001 - program "RESTART").

REFERENCES

[1] M. Faenzi, G. Minatti, D. González-Ovejero, F. Caminita, E. Martini, C. D. Giovampaola, and S. Maci, "Metasurface Antennas: New Models, Applications and Realizations," *Sci Rep*, vol. 9, no. 1, pp. 1–14, Jul. 2019.

[2] G. Minatti, M. Faenzi, E. Martini, F. Caminita, P. De Vita, D. González-Ovejero, M. Sabbadini, and S. Maci, "Modulated Metasurface Antennas for Space: Synthesis, Analysis and Realizations," *IEEE Trans. Antennas Propag.*, vol. 63, no. 4, pp. 1288–1300, Apr. 2015.

[3] G. Minatti, F. Caminita, E. Martini, M. Sabbadini, and S. Maci, "Synthesis of Modulated-Metasurface Antennas With Amplitude, Phase, and Polarization Control," *IEEE Trans. Antennas Propag.*, vol. 64, no. 9, pp. 3907–3919, Sep. 2016.

[4] M. Bodehou, C. Craeye, E. Martini, and I. Huynen, "A Quasi-Direct Method for the Surface Impedance Design of Modulated Metasurface Antennas," *IEEE Trans. Antennas Propag.*, vol. 67, no. 1, pp. 24–36, Jan. 2019.

[5] S. Pearson and S. V. Hum, "Optimization of Electromagnetic Metasurface Parameters Satisfying Far-Field Criteria," *IEEE Trans. Antennas Propag.*, pp. 1–1, 2021.

[6] M. Zucchi, F. Vernì, M. Righero, and G. Vecchi, "Current Based Automated Design of Realizable Metasurface Antennas With Arbitrary Pattern Constraints," *IEEE Trans. Antennas Propag.*, vol. 71, no. 6, pp. 4888–4902, Jun. 2023.

[7] L. Teodorani, M. Zucchi, and G. Vecchi, "Generalized Deterministic Automated Design of Metasurface Antennas with 3D Feeding Structures," *IEEE Trans. Antennas Propag.*, pp. 1–1, 2024.

[8] C. G. Christodoulou, Y. Tawk, S. A. Lane, and S. R. Erwin, "Reconfigurable Antennas for Wireless and Space Applications," *Proc. IEEE*, vol. 100, no. 7, pp. 2250–2261, Jul. 2012.

[9] L. Teodorani, M. Zucchi, and G. Vecchi, "Automated deterministic full design of tensor metasurfaces for field manipulation," May 2025. [Online]. Available: http://dx.doi.org/10.36227/techrxiv.174783897.75656902/v1

[10] I. Lindell, A. Sihvola, and I. Hanninen, "Perfectly anisotropic impedance boundary," *Antennas Propag. IET Microw.*, vol. 1, no. 3, pp. 561–566, Jun. 2007.

[11] S. Rao, D. Wilton, and A. Glisson, "Electromagnetic scattering by surfaces of arbitrary shape," *IEEE Trans. Antennas Propag.*, vol. 30, no. 3, pp. 409–418, May 1982.

[12] F. Foglia Manzillo, M. Śmierzchalski, L. Le Coq, M. Ettorre, J. Aurinsalo, K. T. Kautio, M. S. Lahti, A. E. I. Lamminen, J. Säily, and R. Sauleau, "A Wide-Angle Scanning Switched-Beam Antenna System in LTCC Technology With High Beam Crossing Levels for V-Band Communications," *IEEE Trans. Antennas Propag.*, vol. 67, no. 1, pp. 541–553, Jan. 2019.